Journal of Applied Polymer Science

# Tailoring the Crystalline Morphologies and Mechanical Properties of High-Density Polyethylene Parts by a Change in the Fluid Flow Pattern Under Gas-Assisted Injection Molding

**Quanping Zhang,[1] Long Wang,[1] Xiaochao Xia,[1] Jianmin Feng,[1] Xiaorong Fu,[2] Mingbo Yang[1]**

[1]State Key Laboratory of Polymer Materials Engineering, College of Polymer Science and Engineering, Sichuan University, Chengdu 610065, People's Republic of China

[2]College of Chemical Engineering, Sichuan University, Chengdu 610065, People's Republic of China

Correspondence to: M. Yang (E-mail: yangmb@scu.edu.cn)

**ABSTRACT:** In this study, an increase in the cooling rate of high-density polyethylene parts was carried out via a change in the fluid flow pattern to introduce gas cooling under a gas-assisted injection-molding process; this was conducive to the retention of orientation chains shaped during the injection stage and further developed into much more oriented crystals. Morphological observation showed that the parts without gas cooling (WOGC) were composed of oriented crystals except the gas channel zone, whereas the parts with gas cooling (WGC) were full of oriented crystals, especially much more interlocking shish-kebab structures in the subskin zone. The WGC parts had a higher degree of orientation than the corresponding zone of the WOGC parts. Although the lower crystallinity, the wider orientation regions, and much more interlocking shish-kebab structures led to considerable increases from 32 and 990 MPa in the WOGC parts to 36 and 1150 MPa in the WGC parts for the yield strength and elastic modulus, respectively. © 2014 Wiley Periodicals, Inc. J. Appl. Polym. Sci. **2014**, *131*, 40349.

**KEYWORDS:** crystallization; mechanical properties; morphology; structure–property relations

Received 19 November 2013; accepted 22 December 2013
**DOI: 10.1002/app.40349**

## INTRODUCTION

The tailoring of the crystallization behavior is very important in that the crystalline morphology of polymer materials is closely related to their physical properties.[1–3] Generally speaking, the semicrystalline polymer parts mainly consist of two distinct crystalline morphologies: spherulite and shish-kebab structures.[4,5] The former is developed under quiescent conditions or weak flow fields, whereas the latter requires intense shear or an elongation flow field. The formation of shish-kebab structures deserves special attention because much more highly oriented structures, that is, the shish kebab, can give rise to a noteworthy enhancement of the polymer parts.[6–9] So, understanding and tailoring the polymer crystallization behavior to improve the performance of the polymer parts is important technologically and attractive scientifically.

It is widely accepted that the morphology in an injection-molded part is the result of a competition among the flow rate, crystallization kinetics, relaxation times, and cooling rate.[10] In the skin zone with the highest shear rate along the thickness direction of the parts, the molecular chains are severely oriented and stretched. The stretched chains facilitate the formation of long fibrillar bundles of molecules. Meanwhile, close to the mold wall, the highest cooling rate contributes to the retention of the oriented structure and rapidly crystallizes. Finally, the oriented crystalline morphology, that is, the shish-kebab structure, is formed.[11,12] Conversely, with a distance from the mold wall, the shear rate in the core zone drops, and a few molecular chains are oriented or stretched. Simultaneously, the quite low cooling rate causes the oriented chains to completely relax. As a result, the subsequent lamellar overgrowth leads to the development of a spherulite structure.[13,14]

On the basis of the nature of injection molding, some new injection-molding technologies have been developed,[15–17] which by means of the introduction of both a high shear rate and a long shear duration, thereby induce the formation of an orientation structure, and the orientation zones are distinctly broadened in the thickness direction of parts. According to the same principle, our group has carried out intensive study on the gas-assisted injection molding (GAIM).[18–20] As a result of the multifluid multiflow imposed on the polymer melt, especially the intense shear field triggered by gas penetration, GAIM parts feature an amazing supermolecular structure that is composed of oriented lamellar, shish kebab, and spherulitic structures and so

on.[19,20] In the meantime, compared with common injection-molding parts, richer orientation structures are found in GAIM parts, and these are bound to improve the performance of the parts.

To further promote the properties of GAIM parts, it is quite necessary to consider the GAIM process again. The polymer melt is successively subjected to the intense shear field caused by short shot and gas penetration. The bulk chains are highly oriented or stretched along the flow direction. Afterward, the stretched or oriented chains are retained or relaxed in the cooling stage and further develop into oriented crystals or spherulites, respectively. To some extent, perhaps the shear field in the GAIM process is strong enough,[21,22] the key problem is how to prevent the relaxation behavior of the oriented chains after gas penetration. In other words, in previous studies, we paid more attention to the formation of oriented chains; however, little work has been done on the stability of oriented chains during the molding process.

In this study, we focused on the stability of oriented chains after gas penetration. To achieve that goal, we modified the mold by linking the gas channel with the outside to control the fluid flow pattern during the GAIM process. First, the high-pressure nitrogen initiated an intense shear field, and then, the polymer chains were oriented or stretched during the gas penetration stage. What is more, the continuous gas injection played a crucial role in the enhancement of the cooling rates of the parts by additional convective heat transfer from the gas channel to the outside, as shown in Figure 1. Consequently, many more stretched or oriented molecular chains could be reserved and further developed into richer orientation structures in the GAIM parts, that is, the shish kebab. The results show that the desired crystalline morphology and excellent mechanical properties of high-density polyethylene (HDPE) parts were easily obtained through the tailoring of the fluid flow pattern during the GAIM process.

## EXPERIMENTAL

### Material

A commercially available HDPE (DGDA 6094), with a density of 0.950 g/cm$^3$ and a melt flow rate of 1.0 g/10 min (190°C/2.16 kg, ASTM D 1238), was supplied by the Fujian Refining & Petrochemical Co., Ltd. (Quanzhou City, Fujian Province, China). The gel permeation chromatography profile of the sample is represented in Figure 2.

### Sample Preparation

An injection-molding machine (Model PS40E5ASE, Nissei Plastic Industrial, Inc., Japan), with a mold instrumented with a constant gas pressure controller (Model: MPC-01, Zhongtuo Co., Ltd., China.), was used for the preparation of GAIM parts. A commercial compressed nitrogen ($N_2$) source was used during the gas penetration process. In this study, the parts prepared by the modified mold (as shown in Figure 1) were named with gas cooling (WGC). For comparison, the parts prepared by the common mold (as shown in Figure 1) were named without gas cooling (WOGC). The key processing parameters used in the GAIM experiments are listed in Table I.

### Scanning Electron Microscopy (SEM)

For morphological observations, the GAIM parts were first cut into segments 5.0 mm in length at the middle of the parts,

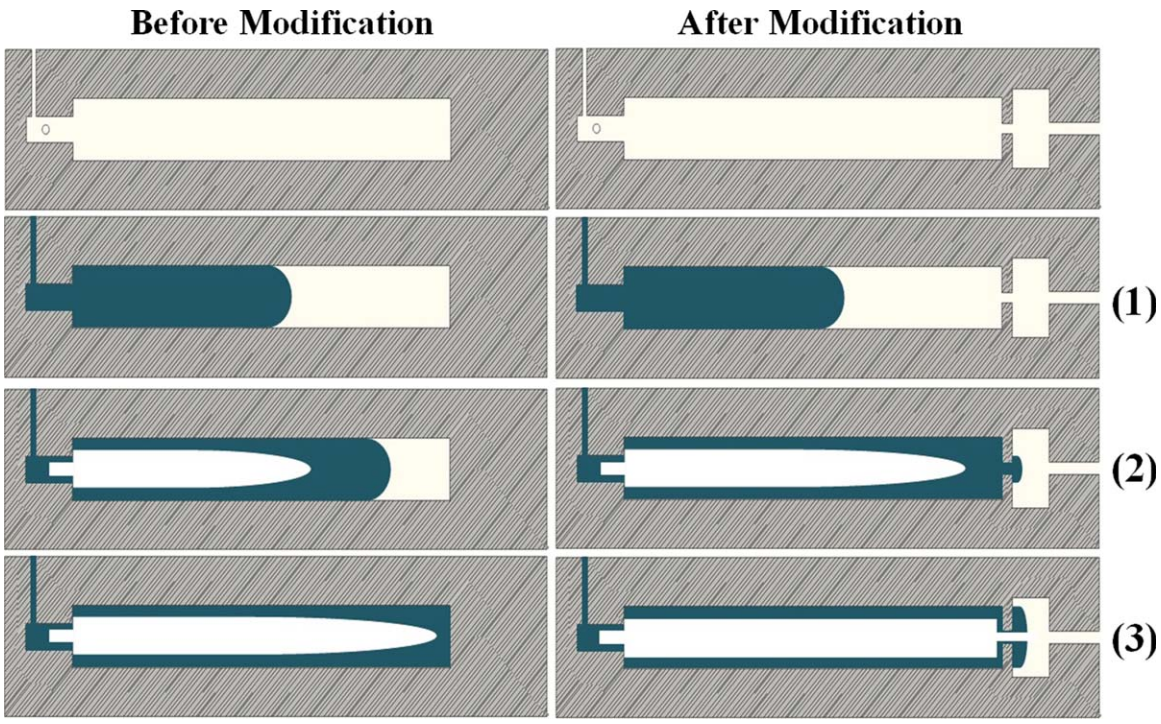


**Figure 1.** Schematic diagram of the GAIM process: (1) melt short shot, (2) gas penetration, and (3) gas packing and cooling stage. [Color figure can be viewed in the online issue, which is available at wileyonlinelibrary.com.]

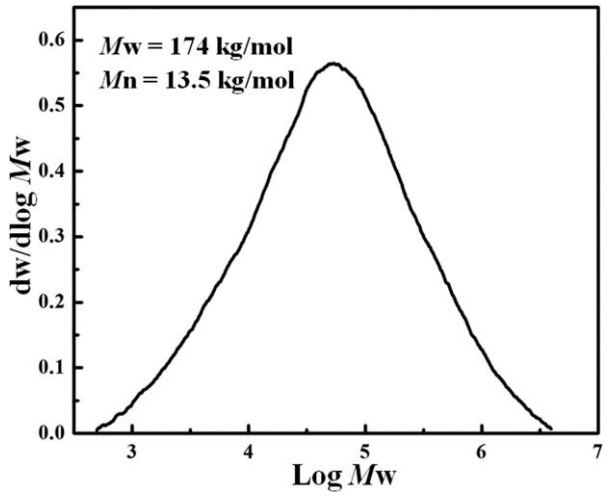


**Figure 2.** Gel permeation chromatography profiles of the HDPE used in this study with 1,2,4-trichlorobenzene as the solvent. The measurements were carried out at 150°C. $M_n$ = number-average molecular weight; $M_w$ = weight-average molecular weight.

subsequently cryogenically fractured in the melt flow direction and then etched by a chemical approach proposed by Olley et al.,[23] as shown in Figure 3. Finally, the surfaces were coated with gold, and the morphologies at different zones of the etched parts were further examined by a scanning electron microscope (model JSM-5900LV, JEOL, Inc., Japan) at an acceleration voltage of 20 kV.

### Two-Dimensional Wide-Angle X-Ray Scattering (2D-WAXS)

The 2D-WAXS experiments were performed on A SEIFERT (DX-Mo8 *0.4-S, 40 kV) diffractometer equipped with a two-dimensional Mar345 CCD X-ray detector; this was in favor of the characterization of the crystal orientation along the thickness direction of the parts. The wavelength of the monochromated X-rays from Cu Kα radiation was 0.154 nm, and the sample-to-detector distance was 425 mm. The 2D-WAXS patterns were obtained every 30 s. The samples were placed with the orientation (flow direction) perpendicular to the projection beams, as described in Figure 3. The Fit-2D software package was used to deal with the resulting 2D-WAXS patterns. The (110) plane of HDPE was examined by the azimuthal scans (0–360°) of 2D-WAXS at a step of 1°. The orientational order parameter ($f$) could be calculated by Herman's orientation function:

$$f = \frac{3\langle\cos^2\varphi\rangle - 1}{2} \quad (1)$$

$$\langle\cos^2\varphi\rangle = \frac{\int_0^{\Pi/2} I(\varphi)\sin\varphi\cos^2\varphi d\varphi}{\int_0^{\Pi/2} I(\varphi)\sin\varphi d\varphi} \quad (2)$$

where $\varphi$ is the azimuthal angle and $I(\varphi)$ is the scattered intensity along the angle $\varphi$. The critical values of $f$, taking $\varphi = 0$ as the shear flow direction, were −0.5 for a perfect perpendicular orientation, 0 for a random orientation, and 1.0 for a perfect parallel orientation.

**Table I.** Processing Parameters of the GAIM Processes

| Processing variable | WOGC | WGC |
|---|---|---|
| Melting temperature (°C) | 200 | 200 |
| Molding temperature (°C) | 30 | 30 |
| Shot size (vol %) | 80 | 80 |
| Injection pressure (MPa) | 100 | 100 |
| Gas pressure (MPa) | 10.4 | 10.4 |
| Gas delay time (s) | 1 | 1 |
| Gas injection time (s) | 20 | 20 |
| Gas temperature (°C) | 10 | 10 |

### Differential Scanning Calorimetry (DSC)

The melt behaviors of different zones of the GAIM parts were carried out under a nitrogen gas flow with a differential scanning calorimeter (model Q-20, TA Instruments) with calibrated indium. Samples of about 5.0 mg inserted into aluminum pans were submitted to heating from 50 to 190°C at a scanning rate of 10°C/min. The crystallinity was calculated from the measured heat of fusion with respect to a perfect crystal heat of fusion of 293.0 J/g.[24]

### Mechanical Testing

Because of the hollow structural characteristics of the GAIM parts, the standard ASTM sample for mechanical testing could not be applied directly. A modified shape of the parts was prepared for tensile testing;[25] this achieved the purpose of qualitative comparison with the tensile properties of the different samples. The tensile tests were performed on an Instron universal testing machine (model 5567) with a crosshead speed of 50 mm/min, and the test temperature was about 20°C.

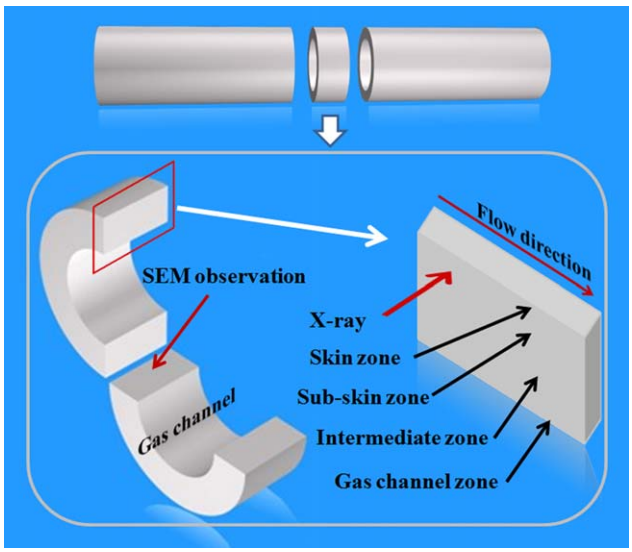


**Figure 3.** Schematic diagram of the structural characterization of the GAIM parts. [Color figure can be viewed in the online issue, which is available at wileyonlinelibrary.com.]

## RESULTS AND DISCUSSION

### Simulation of the Temperature Field during the GAIM Cooling Stage

In our previous studies, the temperature field during the GAIM cooling stage was simulated via a transient heat-transfer model of the enthalpy transformation method and validated in our experiments.[26–29] The parts molded by a common mold were formed simply by a heat conduction method so the parts would mold to the wall during the cooling stage. However, in addition to the mold wall, gas cooling was introduced in the change of the fluid flow pattern during the part cooling stage; this was conducive to enhancing the cooling rate by means of convective heat transfer under the continuous injection of compressed nitrogen though gas channel to the outside. Compared with the previous work, a new parameter, the thermal conductivity of nitrogen ($h$), was seriously considered; this was closely related to the pressure of the nitrogen and the shape of the gas inlet. The specific simulation process will be soon shown in other work. Here, the calculated value of $h$ was about 4700 W $°C^{-1}$ $m^{-1}$. The phase-transition zone of polyethylene started at 119.5°C and ended at 114°C during the cooling stage.[27] The normalized distance was adopted to show the various positions of the parts, that is, $X = 0$ and $X = 1$ represent the skin near the mold surface and the gas channel, respectively.

Figure 4(a) shows the temperature field of the WOGC parts during the cooling stage. The temperature of the position near the mold surface dropped quickly to near the mold temperature. Moreover, an isothermal plateau on the temperature profiles, especially in the inner positions near the gas channel side (e.g., $X = 0.8$–$1.0$), was distinctly displayed. The phase-transition plateau was primarily caused by the rate of heat released from the crystallization process being the same as that taken away by the cold mold.[30,31] From the skin-to-gas channel zone of the parts, the cooling rate was lower closer to the gas channel side.

However, the cooling period of the WGC parts was distinctly different from that of the WOGC parts, as shown in Figure 4(b). As expected, because of the incorporation of gas cooling, the temperature of the gas channel zone was reduced to the phase-transition initial temperature in a shorter time, and the isothermal plateau was turning up. Furthermore, the intermediate zone (e.g., $X = 0.5$–$0.8$) with the lowest cooling rate was compared with the gas channel zone and skin zone at the same time. In other words, gas cooling played a major role in the reduction of the parts' temperature.

Figure 5 shows the temperature profiles at various positions for parts selected; this was in favor of a better comparison of the cooling rates between the WGC and WOGC parts. For WGC or WOGC mode during the cooling stage, the temperature of the parts near the mold wall radically dropped near the mold temperature and solidified as the skin zone. What is more, compared with the WOGC parts, the outset and end position of the phase transition in the intermediate zone and gas channel zone appeared earlier in the cooling curves of the WGC parts during the cooling stage. We could safely conclude that the cooling rate of the WGC parts was much higher than its counterpart.

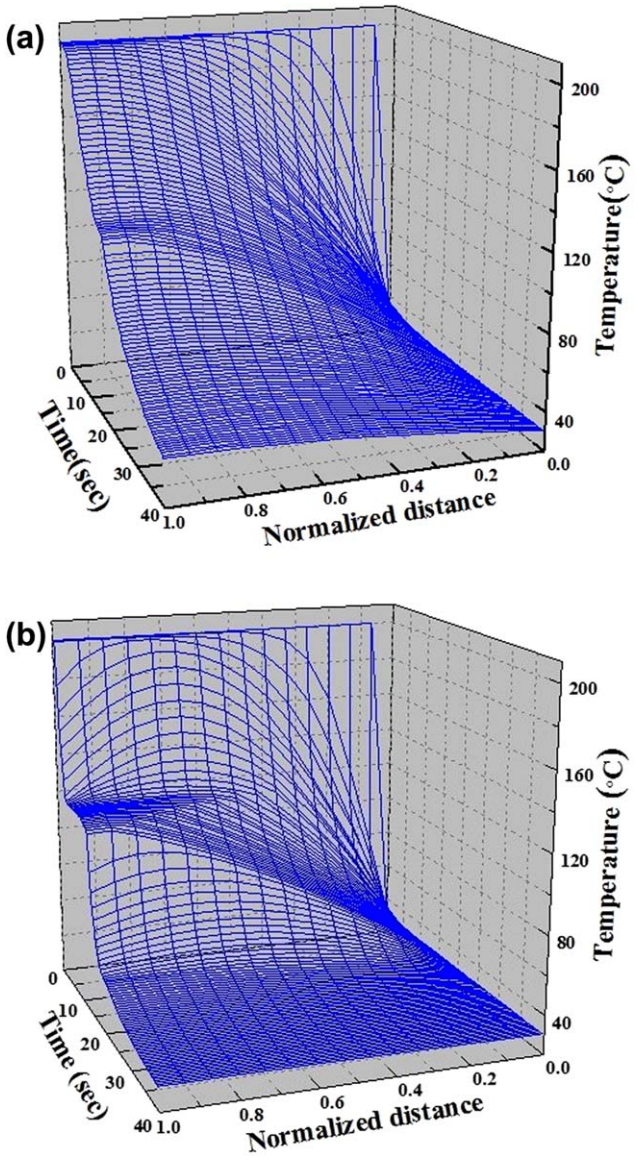


**Figure 4.** Numerical simulation of the temperature distribution of the parts during the cooling stage: (a) WOGC and (b) WGC. [Color figure can be viewed in the online issue, which is available at wileyonlinelibrary.com.]

The polymer melt was successively submitted to the short shot and gas penetration, and this produced an intense shear field during the injection stage, especially in the secondary gas injection stage. The polymer chains were highly stretched or oriented along the flow direction. Afterward, the oriented chains started to relax, and the final chain conformation depended on the cooling rate in the local zone of the parts. The high cooling rate was prone to suppressing the relaxation behavior of the oriented chains and further reserved many more oriented structures. As discussed before, as a result of the cooling rates of the WGC parts being higher than the corresponding zone in the WOGC parts, chain relaxation was restrained, and then, much richer and compact oriented crystals were examined in the WGC parts.

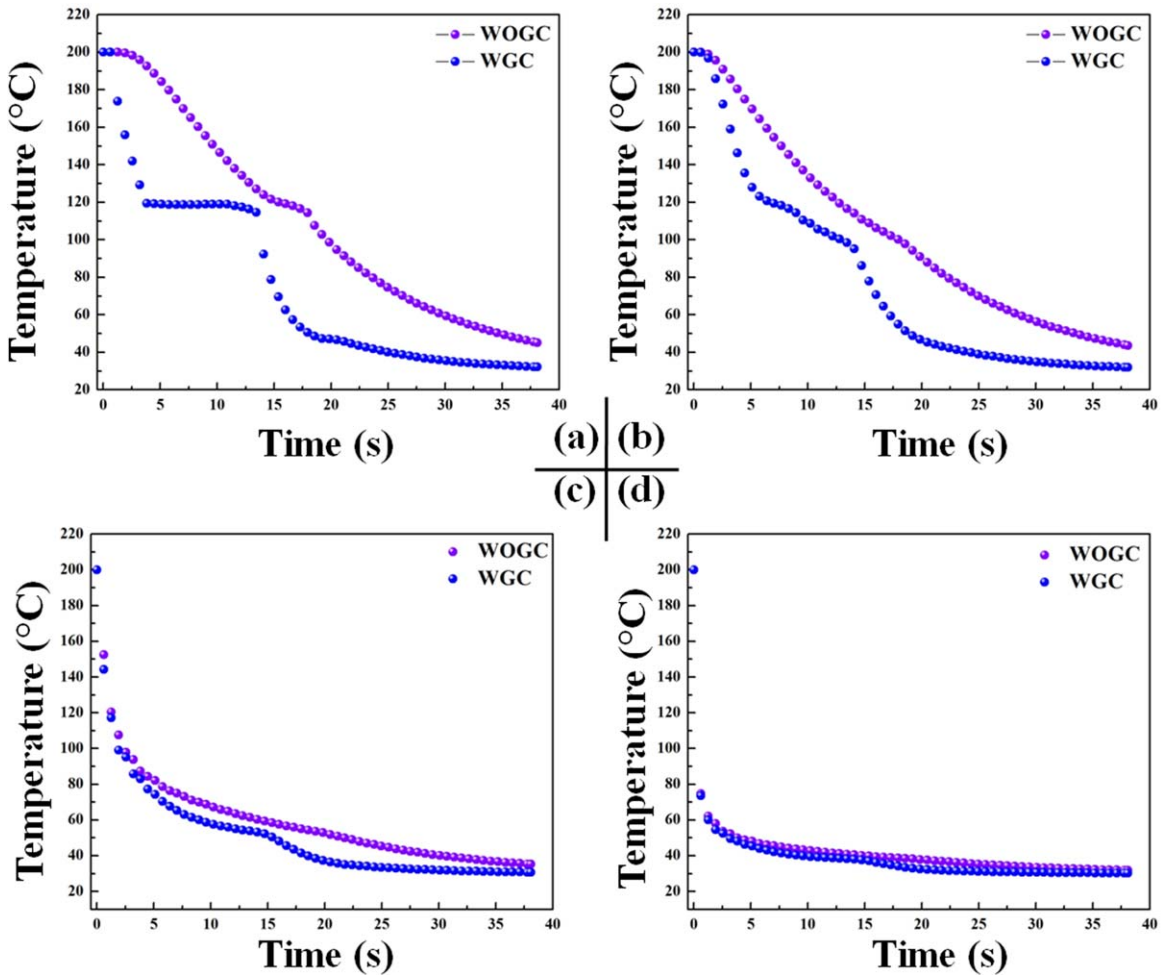


**Figure 5.** Temperature profiles at various part positions: $X$ = (a) 0.95, (b) 0.75, (c) 0.25, and (d) 0.05. [Color figure can be viewed in the online issue, which is available at wileyonlinelibrary.com.]

### Crystalline Morphologies

Figure 6 shows the crystalline morphology of the WOGC parts. First, we clearly observed lots of common spherulitic structures at the gas channel zone ($X = 0.95$) of parts, as presented in Figure 6(a). The absence of the oriented structure could be ascribed to the relatively low shear rate and slow cooling rate; the latter especially provides sufficient time to relax for those orientation chains formed during the gas penetration stage. Second, the crystalline morphology at $X = 0.75$ representing the intermediate zone, as displayed in Figure 6(b), was clearly characterized by the blend structures of oriented lamella and little sizes of spherulite because of the higher cooling rate and shear rate in comparison with the gas channel zone, as described in Figure 6(a). Third, as shown obviously in Figure 6(c), the compacted shish-kebab structures (part interlocking shish kebab) were parallel to the melt flow direction at the position of $X = 0.25$; this represented the subskin zone of parts. In this zone, many more molecular chains were inclined to be highly oriented and stretched under a strong shear field, which was mainly introduced by gas penetration. Unfortunately, even with a high cooling rate, not all of the stretched molecular chains could be retained during the cooling stage in this zone. Then, stretched chains with longer chains develop into highly oriented crystals, that is, shish-kebab structures, whereas the part stretched chains with shorter chain lengths could be relaxed and developed into kebab structures without shish structures during the crystallization process. Finally, as depicted in detail in Figure 6(d), the skin zone of the parts ($X = 0.05$) was packed with oriented lamellas and a few shish-kebab structures shaped during the melt short shot stage.

Figure 7 depicts the crystalline morphology of the WGC parts. Thanks to the incorporation of gas cooling by way of a change in the fluid flow pattern during the GAIM process, many more compact oriented crystals, that is, shish-kebab structures, were obviously discovered in the parts. Moreover, the orientation bands were much broader than the WOGC parts. Above all, as clearly shown in Figure 7(a), a large amount of oriented lamellas instead of the common spherulitic structures were found in the gas channel zone ($X = 0.95$). Even though a few molecular chains were oriented or stretched under the lowest shear rate triggered by the gas penetration in this zone, the relaxation behavior of the oriented chains was effectively retarded via the high cooling rate, as discussed before, so that the part oriented

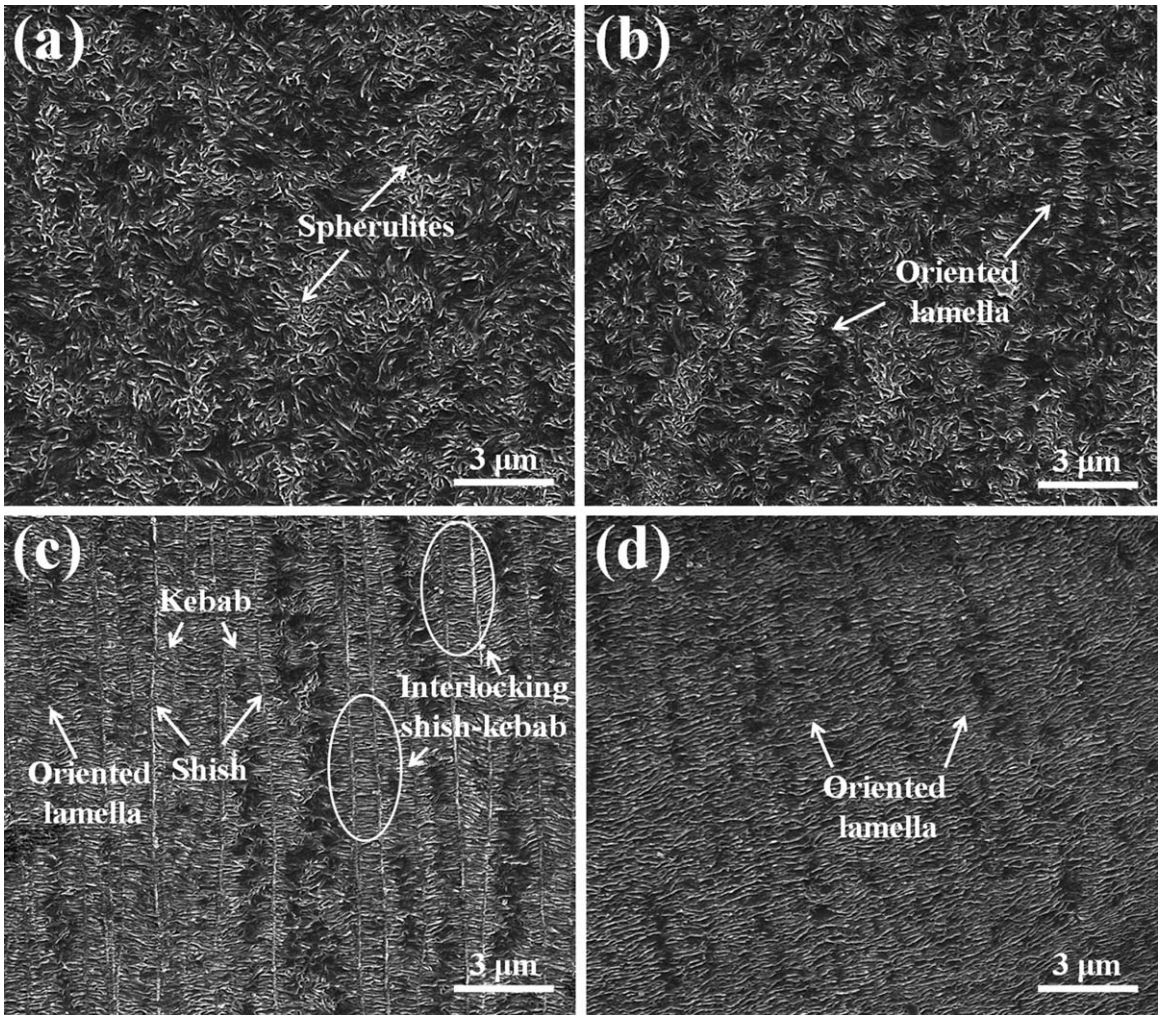


**Figure 6.** Crystalline morphology of the parts WOGC during the cooling stage: $X$ = (a) 0.95, (b) 0.75, (c) 0.25, and (d) 0.05.

chains were reserved and finally developed into oriented lamellas. Furthermore, a good deal of oriented lamellas were clearly found at the intermediate zone ($X = 0.75$) of the parts, as shown in Figure 7(b). Although the cooling rate in this zone was the lowest along the thickness direction, it was still higher than that of the counterparts of the WOGC parts. This resulted in the fact that the cooling time was curtailed, and many more oriented lamellas were shaped. In addition, we distinctly found that at the position ($X = 0.25$) of the parts, as depicted in Figure 7(c), the crystalline morphology was featured by numerous compact, interlocking shish-kebab structures, which tended to improve the mechanical properties.[32] Compared with the WOGC parts in this zone, as a result of the high cooling rate, the cooling stage was shortened, and then, many more oriented or stretched molecular chains were retained. Thereby, the desired crystalline morphology was shaped during the molding process. Finally, blend structures of shish kebab and oriented lamella were clearly observed at $X = 0.05$, as shown in Figure 7(d).

To quantitatively compare the bands of oriented crystals between the WOGC and WGC parts along the thickness direction, the statistical results based on the SEM results are clearly shown in Figure 8. The orientation zone and the highly oriented zone (composed of shish kebabs) of the WGC parts were broader than those of the WOGC parts. To be specific, the WOGC parts were partially occupied by the oriented zone (ca. 76%). Meanwhile, the highly oriented zone was attained at an approximately 54% proportion along the thickness of the parts. However, because of the incorporation of gas cooling via a change in the fluid flow pattern, the orientation structures were clearly detected in almost the whole parts, and the proportion of the highly oriented zone was distinctly increased (from 54 to 68%). These significant differences in the crystalline morphology between the WOGC and WGC parts indicated that the incorporation of gas cooling was very critical to the stability of orientation chains during the GAIM process. With increasing cooling rate by gas cooling, many more oriented or stretched molecular chains were retained; thus, the width of the orientation band in the parts was certainly augmented.

### Molecular Orientation

Figure 9 shows the different orientation behaviors of crystal structures between the WOGC and WGC parts, which were characterized by 2D-WAXS measurements. The inner ring was

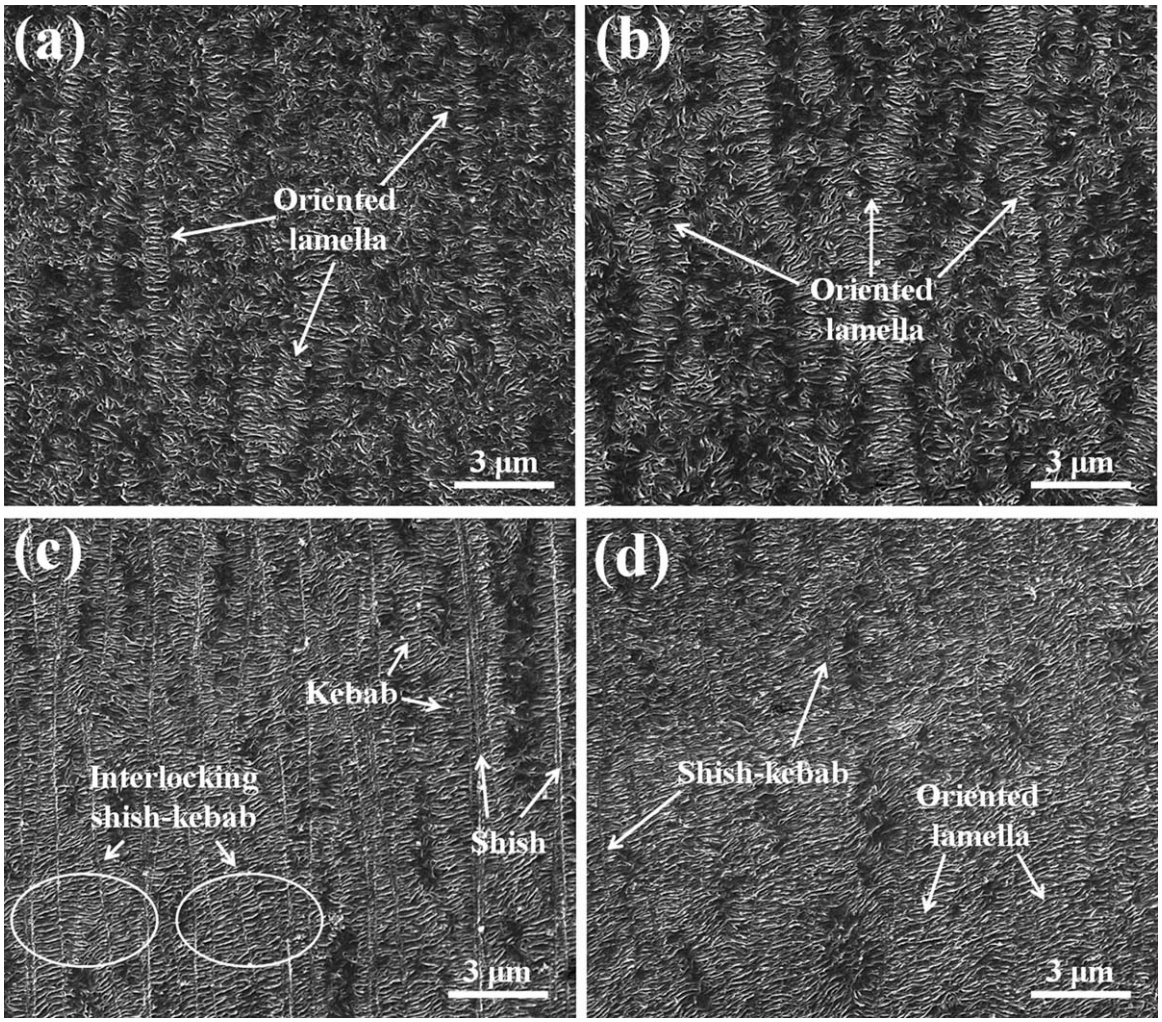


**Figure 7.** Crystalline morphology of the parts WGC during the cooling stage: $X$ = (a) 0.95, (b) 0.75, (c) 0.25, and (d) 0.05.

mean to the (110) lattice planes, whereas the outer ring was represented by the (200) lattice planes. As for the parts WOGC during the cooling stage, the gas channel zone was characterized as an isotropic ring, indicative of a random orientation or low degree of orientation within this zone. In the intermediate zone of the parts, the reflection intensity of the isotropic ring was weaker than that of the gas channel zone; this suggested that a certain number of orientation structures existed in this zone. In the subskin zone, a pair of reflection arcs were seen clearly; this indicated that the crystals were highly oriented along the flow direction. In skin zone, a strong reflection of the (110) plane instead of an isotropic ring was detected in the equatorial direction. This indicated that the crystals were preferentially oriented along the flow direction.

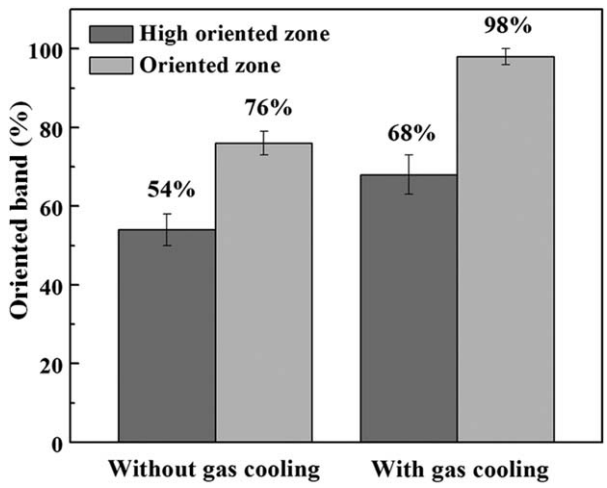


**Figure 8.** Comparison of highly oriented and oriented zones between the WOGC and WGC parts.

Compared with the corresponding zone of the WOGC part, the degree of anisotropy of the WGC parts was much stronger, especially in the gas channel zone with a distinctly anisotropic ring, which was indicative of much more oriented structures in the WGC parts. To better compare the orientation behavior of the crystalline structure among the WGC parts and WOGC parts, the values of the orientation parameters at the corresponding zone for various GAIM parts were obtained, as listed in Table II. The degree of orientation of the WGC parts was higher than that of the WOGC parts in the corresponding zone; this was accordance with the previous SEM results. The polymer

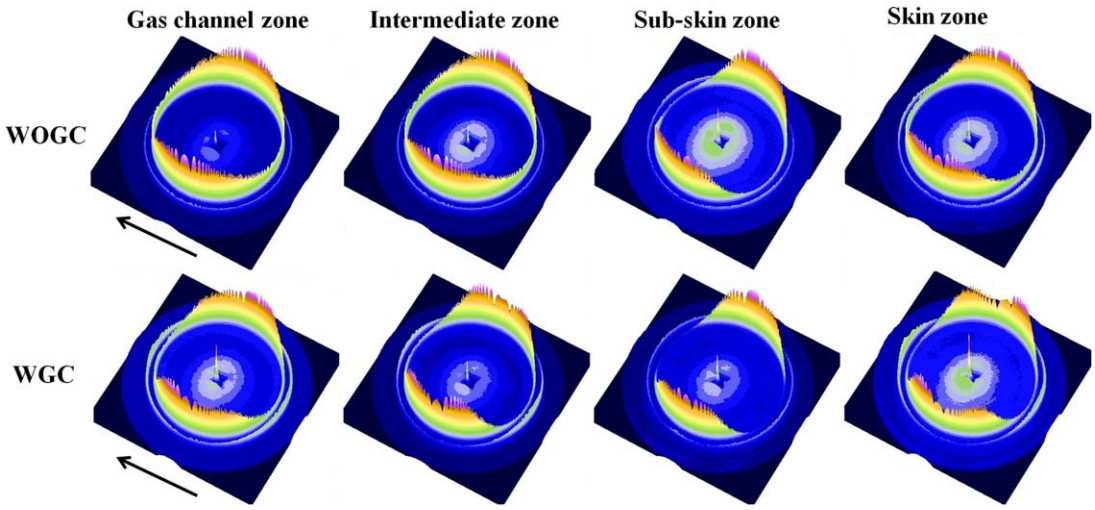


**Figure 9.** 2D-WAXD patterns of the GAIM parts. The direction of the arrow is the flow direction. [Color figure can be viewed in the online issue, which is available at wileyonlinelibrary.com.]

chains of the two type of parts were submitted to an intensity shear field and then oriented or stretched to some extent before the cooling stage during the molding process. The only difference was in the cooling stage; the WGC parts not only relied on the mold wall but also on auxiliary gas cooling, whereas the WOGC parts only depended on mold wall. As expected, because of the incorporation of gas cooling, the cooling rate of the parts was distinctly boosted, and many more oriented or stretched molecular chains were reserved and developed into oriented crystals. Consequently, the degree of orientation of the parts definitely increased.

### Thermal Properties

Figure 10 displays the melting behavior in various zones of the parts, which can indirectly reflect the crystalline morphology. We clearly observed the peak temperature gradually increasing from the skin zone to the gas channel zone for the WOGC parts, whereas the peak temperature increased first and then decreased from the skin zone to the gas channel for the WGC parts. As a result of the lower content of the shish structure compared with the overall crystals in the parts, we could not detect the peak temperature for the shish structure by the DSC equipment; therefore, the curves of the subskin zone for both parts did not have a peak temperature for the shish-kebab structure.[33,34] In addition, the crystallinity for both parts was similar to the tendency of the peak temperature, as listed in Table III. The discrepancy between the WGC and WOGC parts was mainly due to the cooling rate. The cooling rate for the WOGC parts decreased from the skin to the gas channel zone, and thus, the gas channel zone possessed the slowest cooling

**Table II.** Herman's Orientation Factor of the GAIM Parts

| | Gas channel zone | Intermediate zone | Subskin zone | Skin zone |
|---|---|---|---|---|
| WOGC | 0.13 | 0.26 | 0.62 | 0.39 |
| WGC | 0.22 | 0.33 | 0.68 | 0.42 |

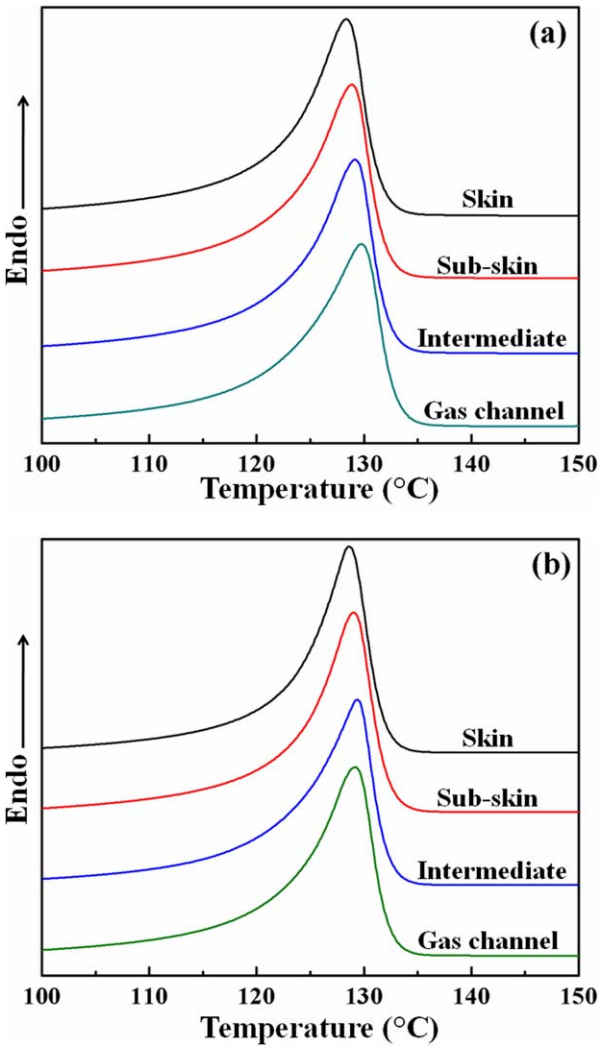


**Figure 10.** DSC heating curves of the GAIM parts: (a) WOGC and (b) WGC. [Color figure can be viewed in the online issue, which is available at wileyonlinelibrary.com.]

**Table III.** DSC Parameters of the GAIM Parts

| | WOGC parts | | | | WGC parts | | | |
|---|---|---|---|---|---|---|---|---|
| Sample location | Skin | Subskin | Intermediate | Gas channel | Skin | Subskin | Intermediate | Gas channel |
| Melting temperature (°C) | 128.7 | 128.9 | 129.2 | 129.8 | 128.7 | 129.0 | 129.1 | 129.3 |
| $X_c$ (%) | 48.4 | 50.7 | 50.9 | 51.2 | 48.4 | 50.6 | 50.8 | 49.5 |

$X_c$ = Crystallinity.

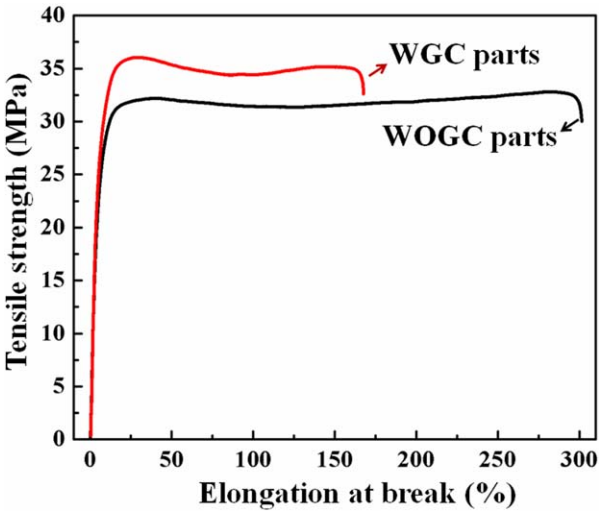


**Figure 11.** Macroscopic tensile behavior of the GAIM parts. [Color figure can be viewed in the online issue, which is available at wileyonlinelibrary.com.]

rate and the longest time for crystallization. However, the high-pressure gas flow pattern was changed by mold modification for the WGC parts, with the result that the cooling rates of the whole parts were largely enhanced, especially the gas channel zone. Consequently, the crystallization process was definitely restrained by the higher cooling rate, and this resulted in relatively imperfect crystals.

### Deformation Behavior

Figure 11 shows the curves of the macroscopic tensile behavior for the WOGC parts and WGC parts. It is shown distinctly that ductile fracture behavior and necking phenomenon occurred for both parts. We observed that the WGC parts had a higher yield stress and elastic modulus and a lower breaking elongation, and the detailed values are listed in Table IV. With regard to the enhancement of the mechanical properties of the WGC parts compared to those of the WOGC parts, on the one hand, a high crystallinity was favorable for enhancing the yield stress and elastic modulus of the parts,[35] but this assumption conflicted with the DSC results. On the other hand, many more shish-kebab structures also affected the mechanical properties. In combination with the SEM results, the WGC parts had a higher yield stress and elastic modulus and a lower breaking elongation. First, this resulted from the formation of richer oriented structures, especially interlocking shish-kebab structures.[32,36] Second, there was another reason for the variation of

**Table IV.** Tensile Testing Results for the GAIM Parts

| Sample | Yield strength (MPa) | Elastic modulus (MPa) | Elongation at break (%) |
|---|---|---|---|
| WOGC parts | 32 ± 0.9 | 990 ± 50 | 290 ± 30 |
| WGC parts | 36 ± 1.5 | 1150 ± 80 | 170 ± 25 |

the mechanical properties that we would like to mention. As shown in Figure 10, almost the whole region along the thickness direction with the orientation structure was further conducive to the promotion of the mechanical properties of the parts.[37,38]

## CONCLUSIONS

In this study, we successfully tailored the crystalline morphology of the GAIM parts and thereby improved the mechanical properties. Because of the change in the fluid flow pattern, the incorporation of gas cooling considerably enhanced the cooling rates and then shortened the cooling stage of the parts; this was in favor of the reservation of many more orientation chains shaped during the gas penetration stage and their further development into various oriented structures, such as shish kebab and oriented lamellae, along the thickness direction. It is worth noting that the richer interlocking shish-kebab structures were formed in the subskin zone of the WGC parts during the molding process. This played an important role in improving the tensile properties of the parts. Consequently, the parts showed much wider regions with compacted orientation crystals and quite a higher degree of orientation than the corresponding zone of the WOGC parts. Therefore, the WGC parts had excellent mechanical properties with a desired superstructure despite the lower crystallinity. On the basis of this study, we were convinced that the control fluid flow pattern in the molding process played an essential role in tailoring the microstructure of the parts; this affected the final performance and deserves more attention.

## ACKNOWLEDGMENTS

The authors express their sincere thanks to Chao-Liang Zhang and Guo-Qiang Pan (National Synchrotron Radiation Laboratory, University of Science and Technology of China) for the SEM and 2D-WAXS experiments, respectively. In addition, the authors acknowledge the National Natural Science Foundation of China for its financial support (contract grant numbers 21174092 and 51121001).

## REFERENCES


1. Kristiansen, M.; Werner, M.; Tervoort, T.; Smith, P.; Blomenhofer, M.; Schmidt, H. W. *Macromolecules* **2003**, *36*, 5150.
2. Housmans, J.; Gahleitner, M.; Peters, G. W. M.; Meijer, H. E. H. *Polymer* **2009**, *50*, 2304.
3. Balzano, L.; Rastogi, S.; Peters, G. W. M. *Macromolecules* **2009**, *42*, 2088.
4. Somani, R. H.; Yang, L.; Zhu, L.; Hsiao, B. S. *Polymer* **2005**, *46*, 8587.
5. Mykhaylyk, O. O.; Chambon, P.; Impradice, C.; Fairclough, J. P. A.; Terrill, N. J.; Ryan, A. J. *Macromolecules* **2010**, *43*, 2389.
6. Sousa, R. A.; Reis, R. L.; Cunha, A. M.; Bevis, M. J. *J. Appl. Polym. Sci.* **2003**, *89*, 2079.
7. Housmans, J. W.; Gahleitner, M.; Peters, G. W. M.; Meijer, H. E. H. *Polymer* **2009**, *50*, 2304.
8. Balzano, L.; Rastogi, S.; Peters, G. W. M. *Macromolecules* **2008**, *41*, 399.
9. Kimata, S.; Sakurai, T.; Nozue, Y.; Kasahara, T.; Yamaguchi, N.; Karino, T.; Shibayama, M.; Kornfield, J. A. *Science* **2007**, *316*, 1014.
10. Janeschitz Kriegl, H. Crystallization Modalities in Polymer Melt Processing: Fundamental Aspects of Structure Formation; Springer: Wien, **2009**; Chapter *3*, p 107.
11. Balzano, L.; Kukalyekar, N.; Rastogi, S.; Peters, G. W. M.; Chadwick, J. C. *Phys. Rev. Lett.* **2008**, *100*, 048302.
12. Kumaraswamy, G.; Verma, R. K.; Issaian, A. M.; Kornfield, J. A.; Hsiao, B. S.; Olley, R. H. *Polymer* **2000**, *41*, 8931.
13. Schultz, J. M. Polymer Crystallization: The Development of Crystalline Order in Thermoplastic Polymers; American Chemical Society: Washington, DC, **2001**.
14. Xu, J. N.; Johnson, M.; Wilkes, G. L. *Polymer* **2004**, *45*, 5327.
15. Kalay, G.; Bevis, M. J. *J. Polym. Sci. Part B: Polym. Phys.* **1997**, *35*, 415.
16. Silva, C. A.; Viana, J. C.; Cunha, A. M. *Macromol. Mater. Eng.* **2007**, *292*, 655.
17. Liu, X. H.; Zhang, C. Y.; Dai, K.; Zheng, G. Q. *Polym. Adv. Technol.* **2013**, *24*, 270.
18. Zheng, G. Q.; Huang, L.; Yang, W.; Yang, B.; Yang, M. B.; Li, Q.; Shen, C. Y. *Polymer* **2007**, *48*, 5486.
19. Huang, L.; Yang, W.; Yang, B.; Yang, M. B.; Zheng, G. Q.; An, H. N. *Polymer* **2008**, *49*, 4051.
20. Sun, N.; Yang, B.; Wang, L.; Feng, J. M.; Yin, B.; Zhang, K.; Yang, M. B. *Polym. Int.* **2012**, *61*, 622.
21. Hu, S.; Yang, W.; Liang, S. P.; Yang, B.; Yang, M. B. *J. Macromol. Sci. Phys.* **2009**, *48*, 1084.
22. Zheng, G. Q.; Yang, W.; Huang, L.; Li, Z. M.; Yang, M. B.; Yin, B.; Li, Q.; Liu, C. T.; Shen, C. Y. *J. Mater. Sci.* **2007**, *42*, 7275.
23. Shahin, M. M.; Olley, R. H.; Blissett, M. J. *J. Polym. Sci. Part B: Polym. Phys.* **1999**, *37*, 2279.
24. Wunderlich, B. In Integration of Fundamental Polymer Science and Technology; Lemstra, P. J. L., Kleinjiens, A., Eds.; Elsevier: London, **1991**; Chapter *3*, p 34.
25. Wang, L.; Yang, B.; Yang, W.; Sun, N.; Zhang, K.; Feng, J. M.; Yang, M. B. *Colloid Polym. Sci.* **2012**, *290*, 1133.
26. Wang, L.; Yang, M. B.; Zhang, Q. P.; Zhang, R. Y.; Wu, J. J.; Feng, J. M. *Polym. Adv. Technol.* **2013**, *24*, 541.
27. Yang, B.; Fu, X. R.; Yang, W.; Huang, L.; Yang, M. B.; Feng, J. M. *Polym. Eng. Sci.* **2008**, *48*, 1707.
28. Yang, B.; Fu, X. R.; Yang, W.; Liang, S. P.; Hu, S.; Yang, M. B. *Polym. Eng. Sci.* **2009**, *49*, 1234.
29. Yang, B.; Fu, X. R.; Yang, W.; Liang, S. P.; Sun, N.; Hu, S.; Yang, M. B. *Macromol. Mater. Eng.* **2009**, *294*, 336.
30. Kamal, M. R.; Lafleur, P. G. *Polym. Eng. Sci.* **1984**, *24*, 692.
31. Supaphol, S.; Spruiell, J. E. *J. Polym. Sci. Part B: Polym. Phys.* **1998**, *36*, 681.
32. Yang, H. R.; Lei, J.; Li, L. B.; Fu, Q.; Li, Z. M. *Macromolecules* **2012**, *45*, 6600.
33. Keum, J. K.; Zuo, F.; Hsiao, B. S. *Macromolecules* **2008**, *41*, 4766.
34. Yang, J. H.; Wang, C. Y.; Wang, K.; Zhang, Q.; Du, R. N.; Fu, Q. *Macromolecules* **2009**, *42*, 7016.
35. Oral, E.; Malhi, A. S.; Muratoglu, O. K. *Biomaterials* **2006**, *27*, 917.
36. Fan, Y.; Lu, Y. C.; Lou, J.; Tang, C. C.; Shinozaki, D. M. *J. Appl. Polym. Sci.* **2013**, *127*, 1387.
37. Shinohara, Y.; Yamazoe, K.; Sakurai, T.; Kimata, S.; Maruyama, T.; Amemiya, Y. *Macromolecules* **2012**, *45*, 1398.
38. Rybnikar, F.; Kaszonyiova, M.; Cermak, R.; Habrova, V.; Obadal, M. *J. Appl. Polym. Sci.* **2013**, *128*, 1665.